2023

Mitochondrial Metabolism in Blood More Reliably Predicts Whole-Animal Energy Needs Compared to Other Tissues

Stefania Casagrande
Evolutionary Physiology Research Group, scasagrande@orn.mpg.de

Maciej Dzialo

Lisa Trost
Max Planck Institute for Ornithology

Kasja Malkoc

Edyta T. Sadowska
Jagiellonian University, Poland

See next page for additional authors

Recommended Citation

Casagrande, S., Dzialo, M., Trost, L., Malkoc, K., Sadowska, E.T., Hau, M., Pierce, B., McWilliams, S., Bauchinger, U. (2023). Mitochondrial metabolism in blood more reliably predicts whole-animal energy needs compared to other tissues, ISCIENCE. Doi: 10.1016/ j.isci.2023.108321.

Journal Pre-proof

Mitochondrial metabolism in blood more reliably predicts whole-animal energy needs compared to other tissues

Stefania Casagrande, Maciej Dzialo, Lisa Trost, Kasja Malkoc, Edyta Teresa Sadowska, Michaela Hau, Barbara Pierce, Scott McWilliams, Ulf Bauchinger

PII: S2589-0042(23)02398-2

DOI: https://doi.org/10.1016/j.isci.2023.108321

Reference: ISCI 108321

To appear in: *ISCIENCE*

Received Date: 4 July 2023

Revised Date: 18 September 2023

Accepted Date: 20 October 2023

Please cite this article as: Casagrande, S., Dzialo, M., Trost, L., Malkoc, K., Sadowska, E.T., Hau, M., Pierce, B., McWilliams, S., Bauchinger, U., Mitochondrial metabolism in blood more reliably predicts whole-animal energy needs compared to other tissues, *ISCIENCE* (2023), doi: https://doi.org/10.1016/j.isci.2023.108321.

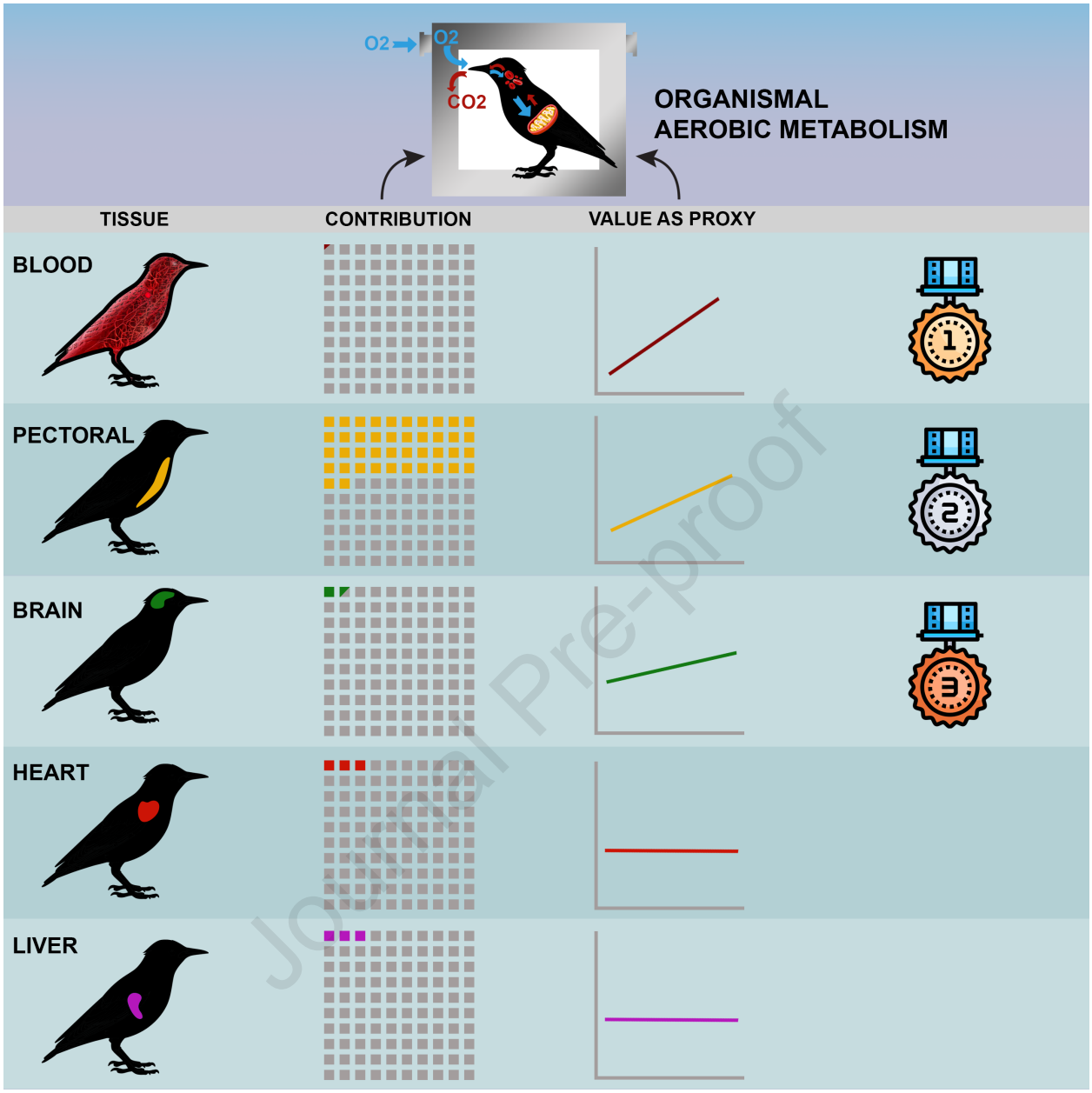

Mitochondrial metabolism in blood more reliably predicts whole-animal energy needs compared to other tissues

Stefania Casagrande[1*°], Maciej Dzialo[2], Lisa Trost[3], Kasja Malkoc[1], Edyta Teresa Sadowska[2], Michaela Hau[1,4], Barbara Pierce[5], Scott McWilliams[6] and Ulf Bauchinger[2,7]

1. Max Planck Institute for Biological Intelligence, Evolutionary Physiology Group, 82319 Seewiesen, Germany.
2. Jagiellonian University, Institute of Environmental Sciences, 30-387 Kraków, Poland
3. Max Planck Institute for Biological Intelligence, Department for Behavioral Neurobiology, 82319 Seewiesen, Germany
4. University of Konstanz, Department of Biology, D-78464 Konstanz, Germany.
5. Sacred Heart University, Department of Biology, Fairfield, CT 06825, USA
6. University of Rhode Island, Department of Natural Resources Science, Kingston, RI 02881, USA
7. Nencki Institute of Experimental Biology, PAS, 02-093 Warsaw, Poland

° Corresponding author: Eberhard-Gwinner-Strasse, 82319 Seewiesen, Germany
E-Mail: stefania.casagrande@bi.mpg.de - Phone: +49 8157 932-248
*Lead contact

Summary

Understanding energy metabolism in free-ranging animals is crucial for ecological studies. In birds, red blood cells (RBCs) offer a minimally invasive method to estimate metabolic rate (MR). In this study with European starlings *Sturnus vulgaris*, we examined how RBC oxygen consumption relates to oxygen use in key tissues (brain, liver, heart, and pectoral muscle) and versus the whole-organism measured at basal levels. The pectoral muscle accounted for 34-42% of organismal MR, while the heart and liver, despite their high mass-specific metabolic rate, each contributed 2.5-3.0% to organismal MR. Despite its low contribution to organismal MR (0.03-0.04%), RBC MR best predicted organismal MR (r=0.70). Oxygen consumption of the brain and pectoralis was also associated with whole-organism MR, unlike that of heart and liver. Overall, our findings demonstrate that the metabolism of a systemic tissue like blood is a superior proxy for organismal energy metabolism than other tissues.

Introduction

The rate at which organisms expend energy relates to species-specific differences in their life history traits and to their ecology [1–6]. Energy expenditure of organisms also flexibly responds to environmental change and this often underlies fundamental differences in individual-level performance [7–10]. Energy metabolism is traditionally assessed by measuring whole-organism oxygen, carbon dioxide or water exchange [5], even though it has long been recognized that energy production and consumption occur within cells of tissues and organs. Yet, tissues differ in metabolic rate and contribution to whole-organism metabolism and performance [11]. Measuring cellular energetics from very small biological samples offers a unique possibility to quantify respiration rates within cells, where aerobic metabolism actually occurs [11–14]. In aerobic eukaryotes, the majority of ATP (adenosine tri-phosphate) molecules that are used to fuel vital functions, are produced in the mitochondria, by coupling molecular oxygen use to ATP production in the process of oxidative phosphorylation. ATP is a molecule that serves as the primary energy currency for cells and it is used to promote chemical reactions that require energy to proceed (e.g. biosynthesis of proteins, cell growth or muscular work). Alterations in the efficiency of aerobic metabolism (i.e. in mitochondrial respiration) to produce ATP to power biological work can have a major impact on the performance and survival of individuals. Because the magnitude of mitochondrial respiration varies widely across tissues due to their divergent metabolic roles [15,16], cellular bioenergetics has been studied mainly in tissues directly involved in supporting energetically costly tasks, such as physical work (e.g. skeletal and cardiac muscles), neurological processes (brain), or vital physiological functions (liver, kidney) [11,17].

Because of the invasiveness of measuring metabolic rate in tissues with high metabolic rate, information derived from mitochondrial bioenergetics measured in peripheral blood has received increasing attention [11]. However, only a few studies have been conducted that directly assess how blood metabolism relates to tissue-specific metabolism. For example, in primates, including humans, monocyte and platelet basal metabolic rates were correlated with ATP-dependent metabolic rate - i.e. oxidative phosphorylation, which accounts for 75-85 % of mitochondrial metabolism [18] of skeletal muscles [19–21]. In addition, monocyte maximal respiration was correlated with maximal respiration of mitochondria isolated from the brain frontal cortex [15,16]. In humans, platelet bioenergetics reflects mitochondrial basal respiration of airway epithelial cells [22]. These studies, carried out in mammals, could not consider RBC aerobic metabolism because mammalian RBCs lack mitochondria and rely on anaerobic glycolysis to produce ATP [23,24]. For all vertebrates, RBCs carry out their well-known passive function of oxygen transport and carbon dioxide elimination, but their ability to produce ATP is less recognized even though RBCs have to carry out processes that require ATP [23,25]. Among these processes are the maintenance of the electrolyte gradient between plasma and RBC cytoplasm, the

synthesis of glutathione and other metabolites for regulating the systemic redox system, the synthesis of metabolites like purine and pyrimidine, the control of systemic nitric oxide levels, the maintenance of systemic pH balance, the modulation of certain immune responses, and, in non-mammalian species, the expression of genes and the synthesis of proteins [23,25]. ATP also serves as the primary energy source for maintaining the structural integrity of RBCs, which is needed to optimize gas exchange [26]. That the physiological processes occurring in blood cells reflect the functioning of the whole organism is of major interest in humans because of the implications in the field of diagnostics. Along these lines, a transcriptomics study showed that more than 80% of the genes expressed in nine distinct human tissue types are co-expressed in peripheral blood [27]. Although the precise mechanisms underlying how physiological processes occurring in blood cells mirror the overall functioning of the whole organism remain uncertain (in [27] blood gene expression is named "illegitimate transcriptomics"), further study is needed that directly assesses how blood metabolism relates to tissue-specific as well as whole-organism metabolism.

Recent studies have provided some evidence that mitochondria in blood cells (platelets, lymphocytes, monocytes, and non-mammalian RBCs) respond to changes in organismal energetic needs [16,19–22,28–37]. For instance, in humans, Liepinsh et al. ([34]) found that individuals with a sedentary lifestyle participating in a bicycle ergometry exercise program enhanced oxidative phosphorylation in blood mononuclear cells by 76% compared to their starting levels. In pied flycatcher (*Ficedula hypoleuca*) females, blood mitochondrial metabolism increased from incubation to chick rearing, thus matching the increased energetic requirements of the parental workload during food provisioning [32]. RBC metabolic rate of great tits (*Parus major*) decreased when individuals shifted from an active to a resting state [38], while it increased in other passerine species in parallel with the higher energy expenditure associated with thermoregulation [39]. Moreover, in garter snakes (*Thamnophis elegans*) of the fast-aging ecotype, blood mononuclear cells show an increase in cellular metabolic rate with advancing chronological age, while the opposite pattern is observed in the slow-aging ecotype [40]. Overall, these studies suggest that blood cell metabolism changes with the energetic needs of the whole organism.

A further step to understand the advantages and the limitations of measuring blood cell metabolism is to investigate to what extent it correlates with whole-organism metabolic rate. Although highly metabolic tissues like muscle and liver consume a significant amount of oxygen, there is no strong evidence to support their use as proxies for overall organismal metabolism. For example, Salin et al. ([41]) found that the organismal metabolic rate in brown trout (*Salmo trutta*) was only associated with liver mitochondrial "proton leak respiration" (LEAK - which is not coupled to ATP production but rather with heat production and accounts for 20-30 % of organismal metabolic rate),

while maximum metabolic rate (which measures the efficiency of the electron transport chain when working at its maximal potential) was associated with muscle mitochondrial LEAK. In contrast, blood has the potential to reflect variation in systemic physiology, like in bioenergetics, telomere dynamics and oxidative stress [20,24,42–47]. Despite this potential, only one study, as far as we know, assessed how RBC metabolic rate relates to organismal metabolic rate [38]. This study showed that organismal metabolic rate of great tits (*Parus major*) was associated with RBC metabolic rate, but only when individuals were not stressed, a physiological state quantified in the study by high circulating levels of glucocorticoids [38]. Since blood has a low metabolic rate (low quantity of oxygen used per time and mass units), compared to other tissues its potential as a proxy for organismal metabolic rate has been neglected, while it could represent a valuable opportunity to unravel how individuals, populations, and species optimize energy expenditure in relation to fitness outcomes.

In this study, we measured the metabolic rate (MR) of the organism (i.e. basal metabolic rate as specified in the methods) as well as that of different tissues (i.e., RBCs, brain, liver, heart and pectoralis muscle) in adult male European starlings (*Sturnus vulgaris*) to assess 1) how much each tissue contributed to organismal MR (see Box 1 for a simplified explanation of the main physiological concepts). We expected 2) that tissue-specific MR, being a systemic tissue in close connection with all the other tissues, can predict organismal MR, and 3) that RBC MR was associated with brain, liver, heart and pectoralis MR. 4) Since the positive association between cell MR and organismal MR can be reversed when birds are stressed [38], we also measured plasma concentrations of corticosterone to control for any metabolic effects associated with the activation of the stress responses [48].

Results

1. How much did each tissue contribute to organismal MR?

Mass-specific MR varied significantly across the tissues tested, with heart fibers exhibiting the highest rate and RBCs the lowest (Table 1; see also Table S1 in the supplement). While the heart muscle had the highest mass-specific metabolic rate, its estimated contribution to the total organismal MRDay was only 2.55%. In contrast, the pectoral muscle contributed 34% to the non-mass specific organismal MRDay, while blood contributed 0.03%. Further statistical details and among-tissue contrasts can be found in Table 1 and Table S1 in the supplement.

2. Can tissue-specific metabolic rate predict organismal metabolic rate?

RBC MR was strongly positively associated with organismal MRNight and with organismal MRDay (Table 2; Figure 1-A1). Simple correlations corroborated the role of RBC metabolism as a proxy for

organismal MR (RBC MR - organismal MRNight: r=0.7, p<0.0001; RBC MR - organismal MRDay: r=0.6, p=0.0002). We would like to mention that in the analysis of tissue-specific metabolic rate we distinguished between the contribution of Complex I alone as well as in combination with Complex II, finding that for the cardiac muscle, only Complex I MR was related to organismal and RBC MR. Full results and interpretations of results about Complex I are reported in the supplement (Table S3 and S4). Similar to what was found in the association with RBCs, organismal MRs (both night and day) were positively associated with brain MR (Table 2, Figure 1-B1,B2) and with MR of the pectoral muscle (Table 2, Figure 1-E1,E2) while they were not associated with liver or heart MR (Table 2, Figure 1-C1,C2,D1,D2). Simple correlations do not support the use of tissue-specific metabolism for organismal MR (brain MR - organismal MRNight: r=0.3, p=0.04; brain MR - organismal MRDay: r=0.3, p=0.08; heart MR - organismal MRNight: r=0.4, p<0.01; heart MR - organismal MRDay: r=0.3, p<0.01; liver MR - organismal MRNight, r=0.1, p=0.67; liver MR - organismal MRDay: r=0.01, p=0.92; pectoral muscle MR - organismal MRNight, r=0.5, p=0.003; pectoral muscle MR - organismal MRDay, r=0.4, p=0.008).

3. Is RBC MR associated with MR of brain, liver, heart and pectoralis?

RBC MR was positively associated with pectoral muscle MR (Table 3, Figure 2-D1) and with brain MR (Table 3, Figure 2-A1), while it was not associated with liver or heart MR (Table 3, Figure 2-B1,C1).

4. Are baseline corticosterone concentrations predicting organismal and tissue-specific MR?

Circulating corticosterone concentrations predicted liver MR (Table 4), but were not related to any of the other metabolic traits considered at the organismal or tissue level (Table 4).

Discussion

Tissue-specific MR of RBC was more strongly associated with whole-organism MR than that of the other four tissues (i.e., brain, pectoralis, liver and heart), suggesting that blood can represent better than other tissues the metabolic rate of the organism. Ours is among the few bird studies that have quantified the metabolic contribution of different tissues to whole-organism MR. We found that mass-specific metabolic rate of starlings was highest in the heart (106.16 pmol $O_2 \cdot s^{-1} \cdot mg^{-1}$) and pectoral muscle (86.49 pmol $O_2 \cdot s^{-1} \cdot mg^{-1}$), followed by liver (56.07 pmol $O_2 \cdot s^{-1} \cdot mg^{-1}$), brain (31.40 pmol $O_2 \cdot s^{-1} \cdot mg^{-1}$) and RBCs (0.29 pmol $O_2 \cdot s^{-1} \cdot mg^{-1}$). An earlier study on European starlings ([69]) showed a much lower oxygen consumption of the pectoralis (about 0.4 mL O_2*g-1*h-1, approximately equal to 0.11 pmol $O_2 \cdot s^{-1} \cdot mg^{-1}$) in comparison to liver (about 3.5 mL O_2*g-1*h-1, approximately equal to 0.97 pmol $O_2 \cdot s^{-1} \cdot mg^{-1}$), but conditions during the measurement were very different from those in the present study: their tissues were not permeabilized and oxygen concentration was kept at 100% (we

did not provide extra oxygen). We estimated that pectoral muscle MR in starlings accounted for about one-third of organismal MR, while the heart and liver, despite their high mass-specific metabolic rate, each contributed only about 2.5% and the brain and blood accounted for even smaller fractions (1.44% and 0.03%, respectively, Table 1). Birds possess different strategies to minimize their body weight for efficient flight than other vertebrate groups. In humans, organs with the highest metabolic rate such as the liver, heart, and brain explain 70-80% of basal metabolic rate, despite comprising only 5% of total body weight [5,49]. The pectoral muscle in birds has to sustain an extraordinary workload to support the most energetically expensive locomotor activity among vertebrates - flying - and it is possible that even at rest it contributes significantly to organismal MR. Further studies should investigate whether blood metabolic rate is also a good proxy for energy expenditure in birds engaged with their ordinary tasks and in their natural environment (i.e. for field metabolic rate). In this case, blood metabolism would be very helpful because it can describe organismal expenditure without having to use complex procedures that are often difficult to apply, especially in free-ranging animals.

The associations between MR of certain tissues and whole-animal MR that we documented are consistent with other types of evidence reported in birds as well as other vertebrates [20,28]. Specifically, the strong positive association that we found between RBC MR and pectoralis MR is in line with that shown in mononuclear peripheral blood cells of non-human primates [20] and in RBCs of king penguins [28]. Studies that used isolated mitochondria under standardized conditions have reported strong associations among tissues [50]. However, using isolated mitochondria can alter the cell environment, interconnections between organelles, and cell signaling that are crucial for mitochondrial functionality [51]. Therefore, using intact cells, such as RBCs, could be more meaningful for ecological studies [11]. In addition, the respiratory states induced by saturated levels of ADP that we considered when studying tissues other than blood and that are commonly used for both isolated mitochondria and permeabilized tissues, represent artificial conditions that are unlikely to occur during natural physiological processes. We investigated the potential of using intact RBCs, which undergo minimal changes compared to when they are functionally active in the body [51], to study the relationship between RBC MR and organismal MR confirming as done previously in great tits [38]. In Malkoc et al 2021 ([38]), the measurements were taken under other conditions compared to the current one: exclusively during the day by transferring active birds from the aviary to the metabolic chambers, in which birds were alert, had only a brief post-absorptive period, and exhibited significant movement within the chambers. As a result, the quantified organismal metabolism could not be defined as basal metabolic rate (measured at rest, after a relative long post-absorptive state and in thermoneutral conditions) but is more aptly described as a "field metabolic rate at rest". Under these conditions, corticosterone played a pivotal role in influencing the correlation between cell and organismal

metabolic rates. In Malkoc et al. some birds exhibited low hormone levels, staying calm within the chamber and presenting what is categorized as "baseline" corticosterone. In contrast, others activated the HPA axis, resulting in stress-induced corticosterone levels. At such elevated levels, corticosterone binds to the GR receptor, modulating key metabolic shifts due to varying energy requirements across tissues, rendering blood a suboptimal representative of organismal MR. In the current study, the conditions were more stringent. We obtained a robust measure of basal metabolic rate and did not record any instances of stress-induced corticosterone levels. As a result, we did not identify corticosterone as a significant mediator of the cell-organismal metabolic relationship, reaffirming the previous study's findings in non-stressed great tits.

The inclusion of organismal MR measured during the day in addition to MRnight measurements was motivated by our aim to comprehensively assess metabolic patterns across different time points and organismal conditions. Despite conducting measurements of organismal metabolic rate in darkness, the birds displayed an increased metabolic rate when measured during their subjective light phase. This approach allowed us to assess the natural shift to daytime metabolic rate without introducing environmental changes within the chamber that could have affected the birds in various ways, such as stress from sudden light exposure or effects of light waves. Our findings revealed that tissue-specific metabolic rates exhibited consistent associations with metabolic rates measured both at night and during the day, despite the higher metabolic rate observed during the day. These results suggest the robustness of tissue-specific metabolic rates in capturing metabolic variations across diurnal cycles. Examining the overall pairwise associations, it becomes evident that not only RBC MR was associated with organismal metabolism, but also that the metabolic rate of RBCs mirrors the metabolic relationships observed at the organismal level. Specifically, RBC MR was associated with pectoral muscle and brain metabolism which were associated with organismal MR, while it was not associated with liver nor heart metabolic rates, which is turn exhibited any significant association with organismal MR. These results shed light on the metabolic relationships within organisms, emphasizing the importance of examining systemic tissue metabolism in the context of overall organismal metabolic patterns.

Tissue metabolism, while vital for understanding cellular processes, is expected to differ between tissues given their distinct functional roles, which makes it challenging to relate it to whole-organism metabolism. For instance, the lack of an association between liver MR and organismal MR is not surprising, as the sampled individuals were in a post-absorptive, fasted state for about 15 hours. During this time, the liver likely played a crucial role in maintaining blood glucose levels through gluconeogenesis under the effect of, among others, corticosterone [52]. Interestingly, in our study liver metabolism was only predicted by baseline levels of corticosterone, a hormone that also regulates

glucose levels during metabolic stressors like starvation, for example, through gluconeogenesis [53]. The concentrations of corticosterone we found (10.79±1.91 ngmL-1) were far below stress-induced levels in the species [54–56], which are approximately 60 ng*mL^{-1} [57]. In line with this, we did not find any relationship between organismal MR and corticosterone levels, as would be expected if our birds had been stressed [38]. Studying individual tissues becomes crucial for addressing questions related to tissue-specific performance. For instance, investigating carotenoid coloration based on pigment transformation occurring in hepatic cells can be effectively studied in the liver [58]. However, caution should be taken when extending these relationships to life-history traits, such as growth, reproductive success, biological aging, or lifespan.

Predicting whole organism MR is of fundamental interest in ecology and evolution, explained by the overwhelming body of literature estimating physiological energy budget. Our understanding of the 'idling costs' of metabolism is of special interest for obesity and diabetes research in medical fields, both of which bearing a huge socioeconomic dimension in terms of human health and costs of health care. Recent advances on the link between blood components (other than RBCs) and organismal metabolism in humans, and the quantified link between RBC oxygen uptake and whole avian metabolism in the current study provide a novel avenue for the quest to determine metabolic rates. This was commonly approached by puzzling together organ masses as the metabolically active tissues, whether in humans [59,60], in non-human animals [61,62], or even through 'meta-predictive equations' utilizing more than a dozen different structural assessments [63]. Our single-tissue approach provides a novel understanding and predictive power, and we envision that similar research on such relationships in mammals and non-mammalian vertebrates will be an important future research avenue.

Conclusions

Blood, along with the heart and blood vessels, comprises the circulatory system and is responsible for transporting essential metabolic substances such as nutrients, metabolites, and signaling factors throughout the body. It is a complex and dynamic tissue that plays a crucial role in maintaining the physiological and metabolic balance of the body. As a result, blood samples, which can be easily and repeatedly obtained, have become an attractive proxy for assessing the health and well-being of an organism, particularly in the context of diagnostics and monitoring. Recent discoveries in mammals suggest that RBCs serve as an inter-organ communication system, with their metabolic system responding to signals circulating in the blood [64]. One possibility is that the mitochondria of tissues can affect the bioenergetics of other tissues, including blood, by releasing signaling molecules such as "mitokines" [45,65]. Also, the amount of oxygen delivered by the blood to the tissues can directly affect the organism's metabolic rate and the blood is responsible for transporting

nutrients such as glucose, amino acids, and fatty acids to the tissues, which support the metabolic rate of the organism. These characteristics allow blood to respond to systemic signals, potentially explaining the significant association we observed between RBC metabolic rate and tissue/organismal metabolic rate. Our study in starlings supports the use of RBC metabolism as a proxy for organismal metabolic rate, with RBC MR being the strongest predictor of whole-organism oxygen consumption. We also found that different tissues have varying contributions to overall metabolic rate, with the pectoral muscle being the largest contributor. While RBC metabolism cannot fully represent all aspects of organismal performance due to the diversity in the functions of different tissues, it can provide a useful tool for understanding energetic state, adjustments or challenges faced by animals in their environment.

Limitations of the study

In this study, we measured metabolic rates of various tissues, as well as the overall organism, strictly under basal conditions (BMR), ensuring a post-absorptive and resting state for the subjects. While this approach provided invaluable insights into the metabolic dynamics at rest, it also posed a limitation. It remains unclear how the strong observed association between blood metabolism and whole-organism metabolism manifests in non-basal scenarios. Malkoc et al. 2021 ([38]) showed similar results in less restrictive settings, but also when birds were at rest. For instance, it is unclear how this relationship holds when birds are feeding, foraging, or undergoing other activities that require an increase in metabolic energy expenditure. Future studies are crucial to evaluate if blood metabolism can be a reliable proxy for assessing dynamic metabolic performance in animals performing their ordinary tasks.

Author contributions

Study design and conceptualization: SC, MD, UB, ES, LT, KM, SMW, MH, BP. Execution of the experiment: MD; SC, LT and KM; Lab analysis: SC and MD; data processing: MD; Statistical analyses: SC; Writing: SC wrote the first draft, all the co-authors reviewed and edited the manuscript and contributed writing the last version of the manuscript.

Acknowledgments

We are grateful to Susan Forrest for raising the starlings. We also thank the Max Planck Institute for Ornithology (now 'Max Planck Institute for Biological Intelligence'), specifically Jane Didsbury, Stefan Leitner, Barbara Worle, and the entire animal care staff for handling the majority of the animal husbandry responsibilities. The study was supported by the Max Planck Society (MPG) (S.C., L.T., K.M. and M.H.), the Jagiellonian University (M.D. grant for young researchers: N18/MNW/000011 and U.B.; grant n:N18/DBS/000003), the National Science Foundation (NSF) (S.R.M. and B.J.P.; grant n: IOS-1354187), the National Science Foundation of Poland (NCN) (U.B.; OPUS grant n: UMO-2015/19/B/NZ8/ 01394).

Declaration of interests

The authors declare that they have no known competing financial interests or personal relationships that could have influenced the work reported in this paper.

Inclusion and diversity statement

We are committed to promoting diverse and equitable research. One or more of the authors of this paper self-identifies as living with a disability. Our team actively supports gender balance.

Main tables

Table 1. Oxygen consumption measured at the organismal levels and in different tissues and estimate of tissue-specific contribution to organismal metabolic rate measure at night (last column) and during the day (MR=metabolic rate. In brackets: sample size.

Level of measure	Mass (g) of Organism/tissue	Mass specific MR (pmol $O_2 \cdot s^{-1} \cdot mg^{-1}$	Overall MR (pmol $O_2 \cdot s^{-1}$)	Tissue contribution (%) MRday	Tissue contribution (%) MRnight
Organism-day	78.90 (38)	46.87 (38)	3.70E+03	----	----
Organism-night	78.90 (38)	37.90 (38)	2.99E+03	----	----
Pectoralis *	7.20 (38)	86.49 (36)	1.25E+03	33.78	41.81
Heart	0.89 (38)	106.16 (38)	9.45E+01	2.55	3.16
Liver	1.65 (38)	56.07 (38)	9.25E+01	2.50	3.09
Brain	1.69 (38)	31.40 (38)	5.31E+01	1.44	1.78
RBCs**	3.75 (38)	0.29 (38)	1.09E+00	0.029	0.038
Among-tissue average		**56.08 (38)**			

Legend: MR=metabolic rate measured as oxygen consumption per unit of time and mass (when appropriate). Organismal MR has been measured at night (MRnight) and in the day (MRday).
* total pectoral mass for mass-specific calculations was estimated by doubling the mass of the left muscle as reported in the table, as the right pectoralis was not measured;
**mass of RBCs was estimated considering that they represent the 45-50% (average 47.5%) of avian blood, which in turn represents approximately the 10% of a bird's body mass (Samour 2006).

Table 2. Predictions of organism MRnight and MRday by tissue-specific metabolic rates

Tissue	Response variable ~ predictor (R2)	Fixed effects	β[95% CrI]	Random effects	σ^2 [95% CrI]
RBC	**Mod. 1 organismal MR_{night} (0.99)**	Intercept	0.38[0.36,0.40]	Day of sampling	0.11[0.004,0.35]
		RBC MR	**0.50[0.31,0.68]**	Residual	0.52[0.41,0.68]
		Metabolic chamber	-0.08[-0.43,0.27]		
	Mod. 1 organismal MR_{day} (0.65)	Intercept	0.43[0.39,0.46]	Day of sampling	0.16[0.008,0.53]
		RBC MR	**0.57[0.30,0.82]**	Residual	0.74[0.57,0.97]
		Metabolic chamber	**0.85[0.37,0.72]**		
Brain	**Mod. 2.2 organismal MR_{night} (0.46)**	Intercept	0.38[0.34,0.41]	Day of sampling	0.19[0.010,0.55]
		Brain MR	**0.22[0.02,0.51]**	Residual	0.64[0.50,0.90]
		Metabolic chamber	-0.13[-0.56,0.31]		
	Mod. 2.2 organismal MR_{day} (0.27)	Intercept	0.43[0.40,0.48]	Day of sampling	0.18[0.007,0.63]
		Brain MR	**0.32[0.02,0.62]**	Residual	0.88[0.68,1.15]
		Metabolic chamber	**0.79[0.20,1.37]**		
Liver	Mod. 3.2 organismal MR_{night} (0.16)	Intercept	0.38[0.37,0.42]	Day of sampling	0.18[0.008,0.56]
		Liver MR	0.04[-0.21,0.28]	Residual	0.71[0.55,0.92]
		Metabolic chamber	-0.13[-0.56,0.31]		
	Mod. 3.2 organismal MR_{day} (0.01)	Intercept	0.43[0.37,0.47]	Day of sampling	0.20[0.009,0.65]
		Liver MR	0.02[-0.32,0.37]	Residual	0.93[0.73,1.22]
		Metabolic chamber	**0.83[0.21,1,46]**		
Heart	Mod. 4.2 organismal MR_{night} (0.11)	Intercept	0.38[0.36,0.40]	Day of sampling	0.19[0.008,0.55]
		Heart MR	0.03[-0.22,0.28]	Residual	0.70[0.55,0.93]
		Metabolic chamber	-0.11[-0.57,0.36]		
	Mod. 4.2 organismal MR_{day} (0.08)	Intercept	0.43[0.39,0.46]	Day of sampling	0.23[0.01,0.74]
		Heart MR	0.09[-0.24,0.44]	Residual	0.92[0.71,1.21]
		Metabolic chamber	**0.82[0.21,1.41]**		
Pectoralis	**Mod. 5.2 organismal MR_{night} (0.48)**	Intercept	0.38[0.36,0.40]	Day of sampling	0.13[0.006,0.45]
		Pect. MR	**0.31[0.08,0.54]**	Residual	0.66[0.52,0.86]
		Metabolic chamber	-0.18[-0.64,0.28]		
	Mod. 5.2 organismal MR_{day} (0.35)	Intercept	0.43[0.39,0.46]	Day of sampling	0.15[0.007,0.53]
		Pect. MR	**0.42[0.11,0.71]**	Residual	0.86[0.66,1.11]
		Metabolic chamber	**0.75[0.17,1.33]**		

Legend: Estimates of fixed (β) and random (σ2) parameters are shown as posterior probabilities with 95% credible intervals (CrI). Statistically meaningful effects are highlighted in bold.

Table 3. Predictions of tissue-specific metabolic rates by RBC metabolic rate.

Tissue	Model (R2)	Fixed effects	β[95% CrI]	Random effects	σ^2 [95% CrI]
Brain	**Mod 8.2 (0.99)**	**RBC MR**	**0.37[0.06,0.69]**	Day of sampling	0.23[0.009,0.70]
				Residual	0.92[0.73,1.21]
Liver	Mod 9.2 (0.97)	RBC MR	0.15[-0.19,0.48]	Day of sampling	0.17[0.007,0.58]
				Residual	0.99[0.79,1.26]
Heart	Mod 10.2 (0.07)	RBC MR	0.02[-0.34,0.38]	Day of sampling	0.29[0.014,0.79]
				Residual	0.96[0.74,1.25]
Pectoralis	**Mod 11.2 (0.98)**	**RBC MR**	**0.36[0.03,0.68]**	Day of sampling	0.23[0.13,0.75]
				Residual	0.92[0.72,1.20]

Legend: Estimates of fixed (β) and random (σ2) parameters are shown as posterior modes with 95% credible intervals (CrI). Meaningful associations are in bold.

Table 4. Relationships of corticosterone concentrations with organismal and tissue-specific metabolic rates

Tissue	Model (R2)	Fixed effects	β[95% CrI]	Random effects	σ^2 [95% CrI]
Organism	MR_{night}(0.80)	Corticosterone	-0.14[-0.36,0.1]	Day of sampling	0.24[0.01,0.62]
		Metabolic chamber	-0.13[-0.59,0.33]	Residual	0.71[0.54,0.91]
	MR_{day} (0.25)	Corticosterone	-0.12[-0.41,0.19]	Day of sampling	0.21[0.009,0.68]
		Metabolic chamber	**0.81[0.16,1.47]**	Residual	0.91[0.72,1.20]
RBC	MR (0.55)	Corticosterone	-0.25[-0.6,0.08]	Day of sampling	0.50[0.04,0.97]
				Residual	0.83[0.59,1.14]
Brain	MR (0.33)	Corticosterone	-0.16[-0.52,0.18]	Day of sampling	0.35[0.02,0.86]
				Residual	0.94[0.71,1.24]
Liver	**MR (1.00)**	**Corticosterone**	**0.27[0.0,0.61]**	Day of sampling	0.16[0.008,0.57]
				Residual	0.97[0.77,1.26]
Heart	MR (0.78)	Corticosterone	0.10[-0.44,0.24]	Day of sampling	0.25[0.009,0.72]
				Residual	0.97[0.76,1.27]
Pectoralis	MR (0.66)	Corticosterone	-0.20[-0.31,0.42]	Day of sampling	0.38[0.02,0.88]
				Residual	0.94[0.71,1.26]

Legend: Estimates of fixed (β) and random (σ2) parameters are shown as posterior modes with 95% credible intervals (CrI). In bold: meaningful associations.

Figure legends

Box 1. Simplified representation of the gas exchange at the organismal and mitochondrial level to explain the measures obtained in the study. Oxygen is transported by red blood cells through the pulmonary vein to the heart and further distributed by the arteriosus system to all body cells. Within the cells, oxygen is utilized in the final step of cellular respiration occurring in the mitochondria's inner membrane. Oxygen acts as the final electron acceptor in the electron transport chain, where it is coupled with ATP production. Carbon dioxide is released during the process of cellular respiration occurring in the mitochondrial matrix (tricarboxylic acid cycle). The metabolic chamber system detects the oxygen subtraction and the carbon dioxide addition by the bird to the air flux delivered into the chamber. At the mitochondrial level, we measured the oxygen consumption of various tissues, including the brain, liver, heart, and pectoral muscle, as well as of red blood cells. Red blood cells were collected from the venous system, where hemoglobin is oxygen depleted. It should be noted that red blood cells perform multiple functions besides carrying respiratory gases, many of which require ATP (see Introduction and Discussion for further details). In red blood cells of non-mammalian vertebrates, ATP is produced in the mitochondria, while in mammalian red blood cells, which lack mitochondria, ATP is produced through anaerobic glycolysis. This suggests that erythrocytes are capable of separating their oxygen-carrying function from their metabolic function, as shown for birds by Stier et al ([28]).

Figure 1. Relationship between organismal MR measured at night (top) and in the subjective day (bottom) and cell MR, corresponding to ROUTINE in intact RBCs and OXPHOS I+II in permeabilized tissues) of: RBCs (A1-2), brain (B1-2), liver (C1-2), heart (D1-2) and pectoralis (“Pect.”, E1-2).

Figure 2. Relationship between RBC MR (representing ROUTINE) and tissue-specific MR representing OXPHOS I+II) of: brain (A1), liver (B1), heart (C1) and pectoralis (D1).

STAR METHODS

RESOURCE AVAILABILITY

Lead contact

Further information and requests for resources should be directed to and will be fulfilled by the lead contact, Stefania Casagrande (Stefania.casagrande@bi.mpg.de).

Material availability

This study did not generate new unique reagents.

Data and code availability

Section 1. The data associated with this study have been deposited in Mendeley Data under the doi: https://data.mendeley.com/drafts/752nyp5j2n, which will be made publicly available upon publication of this research.

Section 2. This paper does not report original code.

Section 3. Any additional information required to reanalyze the data reported in this paper is available from the lead contact upon request.

EXPERIMENTAL MODEL AND STUDY PARTICIPANT DETAILS

Experimental model: Animal

Species: European starling (*Sturnus vulgaris*)

Origin: Wild-caught and hand-raised in captivity

Sex: male

Age: 5-year-old

Sample size: 38

Housing: Birds were housed in groups of 6-7 individuals in six outdoor aviaries (1.0 × 4.0 × 2.0 m; W × L × H) at the Max Planck Institute for Biological Intelligence (MPIBI), Seewiesen, Germany.

Care: The aviaries were exposed to a natural 14light:10dark cycle throughout the experiment. Irrespective of the treatment, all birds were fed ad libitum with a standard maintenance diet consisting of insect powder, nuts, dried fruit pellets, oils, honey, minerals, and live mealworms provided freshly every day.

Institutional permission: All experimental procedures were carried out under the strict ethical guidelines of animal experimentation laws of the European Union and the Regierung von Oberbayern, license no. ROB-55.2-2532.Vet_02-20-160.

METHODS DETAILS

The birds included in this study were part of a research project in which half of the birds received a diet enriched with antioxidants naturally occurring in the food of the species[57,66]. Starting on October 14th, 2021, we randomly selected two birds per day from two different aviaries and transferred them to the laboratory for overnight measurement of basal metabolic rate via respirometry (at resting, in a post-absorptive state, at thermoneutral conditions of 25 ℃ - see below more details), which we refer to as "organismal MR". More specifically, birds were placed in the metabolic chambers at 18:00. The measurement of oxygen consumption began at 22:00, ensuring that the birds had been fasting for 4 hours and were in a post-absorptive state. This measurement continued until 9:00 the following morning. Organismal MR was measured in two consecutive sessions: a night phase (MRnight), assessed between 22:00-07:14h, and a daytime phase (MRday), assessed between 07:15 and 9:00h. Consequently, the last 2 hours of organismal MR measurements corresponded to the first two hours of the natural light phase of the 14light:10dark cycle experienced in the holding aviary exposed to the natural light. Importantly, we did not turn on the lights during the light-phase to avoid alarming the birds and potentially affecting their metabolism. The oxygen consumption traces were considered valid for the analysis when they were relatively stable. The two separate organismal MR measures, the night and daytime measures, were analyzed separately (see below for further information). After being placed into the metabolic chambers at 18:00, the birds were visited again only at 9:00 of the following day, when two researchers (one per bird), switched on the light in the room, opened the metabolic chambers and collected blood samples (maximum of 300 µL in a heparinized capillary) by venipuncture of the brachial vein within 2.5 minutes of opening the door of the laboratory. We stored the blood samples in heparinized Eppendorf tubes on ice until centrifugation (blood was centrifuged for 10 min at 2000 x g and separated from plasma) and bioenergetics analysis, which occurred within about two hours. We weighed the birds (balance KERN CM 150-1N, Kern & Sohn GmbH, Germany; ±0.1 g) and immediately euthanized them by decapitation. We then immediately dissected the birds, and the wet mass of the whole brain, liver, heart, and left side of the pectoral muscle was weighed using a high-precision electronic balance (5-digit; Sartorius, Göttingen, Germany). The dissections were carried out within 40 minutes from the blood sampling, processing one bird at a time by the same researcher, except for the brains, which were processed simultaneously by two researchers.

Measurement of organismal metabolic rate

For the measurement of organismal MR, a multichannel open-flow respirometry system (FMS, Sable Systems, Las Vegas, NV, USA) was used, with two separate plastic respirometry chambers of approximately 7.2 L volume (15 x 21 x 23 cm, W x L x H). These chambers were specifically designed for the measurement of organismal MR and were free from access to food or water during the experiments. All chambers were placed in a temperature-controlled cabinet (PTC-1 Peltier, Sable systems) maintained at 25 °C, within the thermoneutral zone for starlings[67]. Air intake and outtake were regulated by mass flow controllers (MFS Mass Flow System, Sable Systems) at a flow rate of 1300 ml min-1. Oxygen and CO_2 were analyzed with the integrated respirometry system (FMS, Sable Systems) connected to a computer through a UI3 interface (Sable Systems), and data were recorded continuously using ExpeData software (Sable Systems). A subsample of air was drawn from the chamber at a rate of 150 mL min-1 and dried with a magnesium perchlorate (Anhydrone, J.T. Baker, USA) column. Oxygen and CO_2 levels were monitored sequentially from three channels (an empty reference chamber and two chambers with birds), with alternating measurements regulated by a computer-controlled baselining unit and multiplexer (RM-8, Sable Systems).

For each session, the lowest recording after smoothing in each phase was used as an estimate of metabolic rate. Organismal MR measured as ml O_2*min^{-1} was converted into pmol $O_2 \cdot s^{-1} \cdot$ mg of body $mass^{-1}$ (measure units used for cellular MR) based on the assumption that 1 mL of O_2 contains 44,640,000 pmol of the molecule. Due to a temporary power outage during one night, data from the oxygen channel for two birds were lost. However, O_2 consumption for these birds was calculated based on measured CO_2 values divided by the respiratory quotient of 0.718, the estimated average respiratory quotient for the 36 birds with complete measurements.

Measurement of cell metabolic rate in red blood cells

MR of intact RBCs was measured in duplicate using a high-resolution respirometry system, the O2k Oroboros (Oroboros Instruments, Austria), using the average between the two measurements for the statistical analysis (average coefficient of variation ± standard error: CV = 9.42 ± 1.42%; repeatability: 0.82[0.69,0.92], p<0.001). The measurement protocol followed that of Stier et al., 2017. A volume of 30 µL of RBC pellet was weighed and washed in 0.5 mL of MiR05 buffer. After centrifuging for 5 min at 500 x g, the pellet of cells was resuspended in 2.0 mL of pre-equilibrated MiR05 taken from the respiratory chambers, maintained at 40°C, which is the average body temperature of starlings[68]. Oxygen consumption was recorded following a standard sequential substrate/inhibitor addition protocol (SUIT-003_ceD009, https://wiki.oroboros.at/index.php/SUIT-003; Stier et al. 2017[28] and slightly modified in Casagrande et al. 2020[29]. We recorded four states of cellular metabolism when a steady state of at least 3 minutes was established, namely: (1) Cell metabolic rate - MR (corresponding

to ROUTINE in Stier et al. 2017 [28]), reflecting baseline oxygen consumption driven by endogenous substrates and including proton leak and oxidative phosphorylation (see subsequent points); (2) LEAK (recorded after the addition of Oligomycin, 1 µg · ml^{-1}, an inhibitor of ATP-synthase enzyme), reflecting residual respiration after blocking oxidative phosphorylation; (3) Oxidative phosphorylation – OXPHOS, calculated by subtracting LEAK from cell MR, reflecting oxygen consumption linked to ATP synthesis via oxidative phosphorylation; (4) Electron transfer system - ETS (recorded after sequential titration of the uncoupler carbonyl cyanide 3-chlorophenylhydrazone - CCCP, 1 µmol l-1, which uncouple the electron transport chain with ATP-synthase by creating a conductive pathway across the mitochondrial membrane that allows protons to bypass ATP synthase), reflecting the capacity of the electron transfer pathway alone, without the influence of ADP (Adenosine Di-Phosphate, a precursor of ATP) availability; (5) Residual oxygen consumption - ROX (recorded after the addition of Antimycin A, 5 µmol · l^{-1}, a potent inhibitor of the electron transport chain that specifically targets Complex III cytochrome c reductase), which is the non-mitochondrial respiration that was used to correct all previous states. For the purpose of the present study, only measure 1 was considered, as it is the most suitable for comparison with the metabolic traits measured in permeabilized tissues (see below for further explanations about the permeabilization process, see also Stier et al. 2017). All respiration rates were normalized per sample mass and expressed as pmol O_2 · s^{-1} · mg of RBC^{-1}.

Measurement of cell metabolic rates in brain, liver, heart and pectoral muscle

A small sample of all tissues (mean±s.e.) brain: 2.23 ± 0.11 mg; liver: 2.26 ± 0.15 mg; heart: 2.21 ± 0.09 mg; pectoralis: 2.30 ± 0.10 mg) was taken from the same place in each organ using an automated slicer and controlled as best as possible for mass (measured with a high-precision electronic 5-digit balance; Sartorius, Göttingen, Germany) and shape following[69]. Fibers of pectoral and heart muscle were immersed in ice-cold MiR05 buffer (see above) and separated following Pesta and Gnaiger (2015 ([70])). A sample of wet tissue from each organ was weighed as described for RBCs except the tissue weights were measured after quickly drying the sample on filter paper and then transferred to an ice-cold saponin solution until full permeabilization of the soft tissues (10 min) or fibers (30 min) was achieved. The aerobic metabolism of the sample was then measured by transferring the permeabilized biopsy into a metabolic chamber with MIR05 already equilibrated at 40 °C, as described for the intact RBC protocol. To measure the mitochondria bioenergetics of the tissues, we used the Oroboros Suit_011 (https://wiki.oroboros.at/index.php/SUIT-011), which involved the following steps: 1) LEAK was measured in the absence of adenylates (i.e., ATP, ADP, or AMP) by adding NADH-linked substrates - i.e. glutamate (10 mM) and malate (2 mM); 2) Oxidative phosphorylation dependent on the

functioning of complex I (OXPHOS I) was measured by titration of a saturating concentration of ADP. After this step, cytochrome c (10 µM) was added to assess the integrity of the mitochondrial membrane (the membrane was considered intact if the increase in oxygen consumption after cytochrome c oxidase injection was negligible). Only in two cases (pectoral muscles), oxygen consumption was increased, and the measurements were not considered for the analysis (consequently, data for pectoral muscle has a reduced sample size, see below). 3) Oxidative phosphorylation dependent on the functioning of complex I and II - OXPHOS I+II - was measured by adding succinate (10 mM) to stimulate oxidative phosphorylation at complex II. OXPHOS I+II most closely resembles cell MR measured in intact RBCs because it includes LEAK and oxidative phosphorylation. 4) Maximal capacity of the electron transfer system (ETS), was measured adding the uncoupler CCCP as described for intact RBCs. To further describe the system, we inhibited complex I by rotenone (10 µM) to describe the contribution of complex II alone (these data were not used because not relevant for the purpose of the study). 5) To obtain the residual non-mitochondrial oxygen consumption – ROX - we inhibited complex III with Antimycin, as described for intact RBCs. ROX was subtracted from all respiratory states previously described. The oxygen concentration of the metabolic chambers was kept above 60 pmol of O_2 by opening the chambers to allow full oxygenation when this threshold was reached (specifically just before the addition of the uncoupler CCCP). All measurements were normalized to the mass of the sample analyzed, and expressed as pmol $O_2 \cdot s^{-1} \cdot$ mg of tissue^{-1}. To compare oxygen consumption by organismal, RBCs, and tissue-specific metabolism, we considered only OXPHOS I+II (referring to as “tissue MR”), because this measure includes proton leak and oxidative phosphorylation as well as cell and organismal MR (results including OXPHOS measured in Complex I alone, are reported in Table S3 and S4 in SEM).

Measurement of corticosterone

Plasma corticosterone concentrations were measured using an enzyme immunoassay kit (Arbor Assays, Cat. No. K014-H1). A 15 µL plasma sample was extracted using double diethyl ether extraction, following an established protocol [29]. Specifically, we firstly dilute in glass tubes 10 µL plasma of unknown samples, 8 µL of plasma of controls for low corticosterone concentration (stripped chicken plasma controls with corticosterone added at concentrations of 5 ng mL^{-1}) and 4 µL of plasma of controls for high corticosterone concentration (stripped chicken plasma controls with corticosterone added at concentrations of 10 ng mL^{-1}) in 150 µL of HPLC grade H_2O_2. Two glass tubes contained only HPLC water were taken through the entire procedure to check for unintended hormone contamination. After vertexing each tube, under the fume hood we added 1 mL of diethyl ether and shaked for 10’ at 450 rpm. In the process of isolating the hormone-rich lipophilic phase from the water phase, a temperature-induced phase separation method was employed. Specifically, tubes were

briefly submerged in the ethanol with dry-ice for approximately 30 seconds, ensuring a clear demarcation between the two phases. Following this, the liquid phase was carefully decanted into new tubes. To ensure maximal recovery of the lipophilic phase containing the hormones, the initial tubes were retained and subjected to a repeat of the aforementioned procedure, beginning from the addition of diethyl ether. Between extractions, the tubes from the first extraction were stored under the hood and shielded from light with aluminum wrap. The extraction solution was dried under a nitrogen flow at a controlled temperature of 37°C. Samples were then re-dissolved in 150 µL of assay buffer, thoroughly vortexed, and allowed to reconstitute overnight, after sealing them with parafilm. The assay for corticosterone was conducted in accordance with the kit's protocol, utilizing an 8-point standard curve that ranged from 10 $ng*mL^{-1}$ to 0.78 $ng*mL^{-1}$. The inter-plate coefficient of variation (CV) was calculated using the average and standard deviation of the four controls (high and low concentrations) of the two plates run and was 2.88% for the high control and 5.38% for the low control. The intra-plate CV was calculated as the average CV of the concentrations of the low (2.33±1.15%) and high control (1.88±1.13%), respectively, run on the two plates.

QUANTIFICATION AND STATISTICAL ANALYSIS

All statistical models were fitted using a Bayesian framework implemented in the statistical software R (v. 4.2.2, R Core Team 2022) using the R-package "rstanarm" [71,72]. Duplicate repeatability of RBC MR was computed wit R package "rptR". For all models, we used parameter-flat priors[72]. We ran 4 chains of 4000 iterations each to ensure that the minimum Markov chain Monte Carlo entailed an effective sample size. All models showed absolute autocorrelation values lower than 0.1, satisfied convergence criteria based on the Heidelberger and Welch convergence diagnostics [73] and had an effective sample size ("neff") close to expected iterations, while none had a "rhat" value above 1.02. To assess the distribution of residuals, we used normal quantile-quantile plots, Tukey-Ascombe plots, and plotted residuals against leverage. We drew inferences from the posterior distribution and 95% credible interval (CrI), considering fixed effects to be meaningful if the range 2.5-97.5% CrI did not include zero. When used as covariates, variables were standardized with z-scores, but we report the original values in the graphs for clarity. We checked whether variables met the assumptions of homogeneity of variance and normal distribution by visually analyzing the graphical distributions of fitted values versus their residuals.

In a preliminary analysis, we assessed differences in MRs among tissues and organism using a post-hoc analysis after running a linear mixed model that included mass-specific oxygen consumption as the dependent variable, the type of tissue as a predictor (6 levels: organism, brain, liver, pectoral

muscle, heart, and blood), and individual identity (n=38 except for pectoral muscle, for which n=36) and day of sampling (as the experiment ran over 40 days) as random factors (results reported in Table 1 and Table S1).

To assess whether tissue-specific metabolic rate predicted organism MR (Table 2), we ran models with mass-specific organismal MRnight or MRday (pmol $O_2 \cdot s^{-1} \cdot$ mg of body mass^{-1}) as the dependent variable in separate models. We included mass-specific metabolic rate (pmol $O_2 \cdot s^{-1} \cdot mg^{-1}$) of the tissue of interest as the predictor. We also included the metabolic chamber (2-level fixed factor for both cellular and organismal MR) as a fixed factor to control for any variation between the two environments but this factor was excluded from cellular MR analysis because it did not explain any variance (data not shown), while it was retained for organismal MR because it was meaningful. Since the experiment was run over four weeks, the day of sampling was included as a random effect as in the previous analyses. The best way to correct organismal MR for body mass, since it scales with body mass, is to include body mass as a covariate (McElreath, 2020 [74] where use of residuals in this context is discouraged). However, here we wanted to normalize the oxygen consumption during cell and organismal respiration in the same way (i.e., by dividing oxygen consumption by the mass of interest). Models run in both ways (including body mass as a covariate or correcting metabolic rate for body mass) did not differ substantially (see supplementary material for models with overall organismal MR corrected for body mass included as predictor, Table S2). Since this part of the analysis addressed the major goal of the study, which was to understand whether blood metabolism can be used as a proxy for organismal metabolism, we also provided Pearson's correlation coefficients and relative significant levels (*p*-values), since biomedical research considers a proxy to be valuable if $r \geq 0.6$[75].

We then assessed whether RBC MR could predict tissue-specific MR (Table 3). For this purpose, we ran separate models with MR (=OXPHOS I+II) of each tissue as the dependent variable and RBC MR (=ROUTINE, see methods above) as the covariate. Similar to the previous models, the day of sampling was included as a covariate. The effect of dietary treatment was not considered because all variables and predictors represent post-treatment factors; thus, they already account for any effect of treatment. In other words, adding "treatment" would mean incurring in the so called "post-treatment bias"[74]. This approach is also justified because we were not interested in the effect of treatment, which was not relevant for the purpose of the present study. However, we report the effect of diet treatment on organismal, RBC and tissue-specific MR in Figure S1 of the supplement.

References

1. Brown, J.H., Gillooly, J.F., Allen, A.P., Savage, V.M., and West, G.B. (2004). Toward a metabolic theory of ecology. Ecology *85*, 1771–1789.
2. Glazier, D.S. (2006). The 3/4-power law is not universal: Evolution of isometric, ontogenetic metabolic scaling in pelagic animals. Bioscience *56*, 325–332. 10.1641/0006-3568(2006)56[325:TPLINU]2.0.CO;2.
3. Glazier, D.S. (2015). Is metabolic rate a universal "pacemaker" for biological processes? Biol. Rev. *90*, 377–407. 10.1111/brv.12115.
4. Kozłowski, J., Konarzewski, M., and Czarnoleski, M. (2020). Coevolution of body size and metabolic rate in vertebrates: a life-history perspective. Biol. Rev. *95*, 1393–1417. 10.1111/brv.12615.
5. Metcalfe, N.B., Crespel, A., Hood, W.R., Nadler, L.E., Ozanne, S.E., Bellman, J., Dawson, N.J., Hopkins, M., Bize, P., Dunn, R.E., et al. (2023). Solving the conundrum of intra-specific variation in metabolic rate : A multidisciplinary conceptual and methodological toolkit New technical developments are opening the door to an understanding of why metabolic rate varies among individual animals of a. BioEssays, 1–14. 10.1002/bies.202300026.
6. Pettersen, A.K., White, C.R., and Marshall, D.J. (2016). Metabolic rate covaries with fitness and the pace of the life history in the field. Proc. R. Soc. B Biol. Sci. *283*. 10.1098/rspb.2016.0323.
7. Hudson, L.N., Isaac, N.J.B., and Reuman, D.C. (2013). The relationship between body mass and field metabolic rate among individual birds and mammals. J. Anim. Ecol. *82*, 1009–1020. 10.1111/1365-2656.12086.
8. Réale, D., Garant, D., Humphries, M.M., Bergeron, P., Careau, V., and Montiglio, P.O. (2010). Personality and the emergence of the pace-of-life syndrome concept at the population level. Philos. Trans. R. Soc. B Biol. Sci. *365*, 4051–4063. 10.1098/rstb.2010.0208.
9. Sokolova, I. (2018). Mitochondrial Adaptations to Variable Environments and Their Role in Animals' Stress Tolerance Society for Integrative and Comparative Biology. Integr. Comp. Biol., 1–13. 10.1093/icb/icy017.
10. White, C.R., Marshall, D.J., Alton, L.A., Arnold, P.A., Beaman, J.E., Bywater, C.L., Condon, C., Crispin, T.S., Janetzki, A., Pirtle, E., et al. (2019). The origin and maintenance of metabolic allometry in animals. Nat. Ecol. Evol. *3*, 598–603. 10.1038/s41559-019-0839-9.
11. Koch, R.E., Buchanan, K.L., Casagrande, S., Crino, O., Dowling, D.K., Hill, G.E., Hood, W.R., McKenzie, M., Mariette, M.M., Noble, D.W.A., et al. (2021). Integrating Mitochondrial Aerobic Metabolism into Ecology and Evolution. Trends Ecol. Evol. *36*, 321–332. 10.1016/j.tree.2020.12.006.
12. Gnaiger, E. (2014). Mitochondrial Pathways and Respiratory Control An Introduction to OXPHOS Analysis.
13. Havird, J.C., Shah, A.A., and Chicco, A.J. (2020). Powerhouses in the cold: mitochondrial function during thermal acclimation in montane mayflies. Philos. Trans. R. Soc. B Biol. Sci. *375*, 20190181. 10.1098/rstb.2019.0181.
14. Lane, N., and Martin, W. (2010). The energetics of genome complexity. Nature *467*, 929–934. 10.1038/nature09486.

15. Cardoso, S.M., Santana, I., Swerdlow, R.H., and Oliveira, C.R. (2004). Mitochondria dysfunction of Alzheimer's disease cybrids enhances Aβ toxicity. J. Neurochem. *89*, 1417–1426. 10.1111/j.1471-4159.2004.02438.x.

16. Tyrrell, D.J., Bharadwaj, M.S., Jorgensen, M.J., Register, T.C., Shively, C., Andrews, R.N., Neth, B., Dirk Keene, C., Mintz, A., Craft, S., et al. (2017). Blood-based bioenergetic profiling reflects differences in brain bioenergetics and metabolism. Oxid. Med. Cell. Longev. *2017*. 10.1155/2017/7317251.

17. Spinelli, J.B., and Haigis, M.C. (2018). The multifaceted contributions of mitochondria to cellular metabolism. Nat. Cell Biol. 10.1038/s41556-018-0124-1.

18. Brand, M.D., Brindle, K.M., Buckingham, J.A., Harper, J.A., Rolfe, D.F.S., and Stuart, J.A. (1999). The significance and mechanism of mitochondrial proton conductance. Int. J. Obes. *23*, S4–S11. 10.1038/sj.ijo.0800936.

19. Braganza, A., Annarapu, G.K., and Shiva, S. (2020). Blood-based bioenergetics: An emerging translational and clinical tool. Mol. Aspects Med. *71*, 100835. 10.1016/j.mam.2019.100835.

20. Tyrrell, D.J., Bharadwaj, M.S., Jorgensen, M.J., Register, T.C., and Molina, A.J.A. (2016). Blood cell respirometry is associated with skeletal and cardiac muscle bioenergetics: Implications for a minimally invasive biomarker of mitochondrial health. Redox Biol. *10*, 65–77. 10.1016/j.redox.2016.09.009.

21. Tyrrell, D.J., Bharadwaj, M.S., Van Horn, C.G., Kritchevsky, S.B., Nicklas, B.J., and Molina, A.J.A. (2015). Respirometric Profiling of Muscle Mitochondria and Blood Cells Are Associated With Differences in Gait Speed Among Community-Dwelling Older Adults. Journals Gerontol. - Ser. A Biol. Sci. Med. Sci. *70*, 1394–1399. 10.1093/gerona/glu096.

22. Winnica, D., Corey, C., Mullett, S., Reynolds, M., Hill, G., Wendell, S., Que, L., Holguin, F., and Shiva, S. (2019). Bioenergetic Differences in the Airway Epithelium of Lean Versus Obese Asthmatics Are Driven by Nitric Oxide and Reflected in Circulating Platelets. Antioxidants Redox Signal. *31*, 673–686. 10.1089/ars.2018.7627.

23. Van Wijk, R., and Van Solinge, W.W. (2005). The energy-less red blood cell is lost: Erythrocyte enzyme abnormalities of glycolysis. Blood *106*, 4034–4042. 10.1182/blood-2005-04-1622.

24. Yachie-Kinoshita, A., Nishino, T., Shimo, H., Suematsu, M., and Tomita, M. (2010). A metabolic model of human erythrocytes: Practical application of the E-Cell Simulation Environment. J. Biomed. Biotechnol. *2010*. 10.1155/2010/642420.

25. Kuhn, V., Diederich, L., Keller, T.C.S., Kramer, C.M., Lückstädt, W., Panknin, C., Suvorava, T., Isakson, B.E., Kelm, M., and Cortese-Krott, M.M. (2017). Red Blood Cell Function and Dysfunction: Redox Regulation, Nitric Oxide Metabolism, Anemia. Antioxidants Redox Signal. *26*, 718–742. 10.1089/ars.2016.6954.

26. Betz, T., Lenz, M., Joanny, J.F., and Sykes, C. (2009). ATP-dependent mechanics of red blood cells. Proc. Natl. Acad. Sci. U. S. A. *106*, 15320–15325. 10.1073/pnas.0904614106.

27. Liew, C.C., Ma, J., Tang, H.C., Zheng, R., and Dempsey, A.A. (2006). The peripheral blood transcriptome dynamically reflects system wide biology: A potential diagnostic tool. J. Lab. Clin. Med. *147*, 126–132. 10.1016/j.lab.2005.10.005.

28. Stier, A., Romestaing, C., Schull, Q., Lefol, E., Robin, J.P., Roussel, D., and Bize, P. (2017). How to measure mitochondrial function in birds using red blood cells: a case study in the king penguin and perspectives in ecology and evolution. Methods Ecol. Evol. *8*, 1172–1182. 10.1111/2041-210X.12724.

29. Casagrande, S., Stier, A., Monaghan, P., Loveland, J.L., Boner, W., Lupi, S., Trevisi, R., and Hau, M. (2020). Increased glucocorticoid concentrations in early life cause mitochondrial inefficiency and short telomeres. J. Exp. Biol. *223*, 222513. 10.1242/jeb.222513.

30. Riou, M., Alfatni, A., Charles, A.L., Andres, E., Pistea, C., Charloux, A., and Geny, B. (2020). New insights into the implication of mitochondrial dysfunction in tissue, peripheral blood mononuclear cells, and platelets during lung diseases. J. Clin. Med. *9*. 10.3390/jcm9051253.

31. Rose, S., Carvalho, E., Diaz, E.C., Cotter, M., Bennuri, S.C., Azhar, G., Frye, R.E., Adams, S.H., and Børsheim, E. (2019). A comparative study of mitochondrial respiration in circulating blood cells and skeletal muscle fibers in women. Am. J. Physiol. - Endocrinol. Metab. *317*, E503–E512. 10.1152/AJPENDO.00084.2019.

32. Stier, A., Bize, P., Hsu, B.Y., and Ruuskanen, S. (2019). Plastic but repeatable: Rapid adjustments of mitochondrial function and density during reproduction in a wild bird species. Biol. Lett. *15*, 9–13. 10.1098/rsbl.2019.0536.

33. Stier, A., Bize, P., Schull, Q., Zoll, J., Singh, F., Geny, B., Gros, F., Royer, C., Massemin, S., and Criscuolo, F. (2013). Avian erythrocytes have functional mitochondria, opening novel perspectives for birds as animal models in the study of ageing. Front. Zool. *10*, 1–9. 10.1186/1742-9994-10-33.

34. Liepinsh, E., Makarova, E., Plakane, L., Konrade, I., Liepins, K., Videja, M., Sevostjanovs, E., Grinberga, S., Makrecka-Kuka, M., and Dambrova, M. (2020). Low-intensity exercise stimulates bioenergetics and increases fat oxidation in mitochondria of blood mononuclear cells from sedentary adults. Physiol. Rep. *8*, 1–11. 10.14814/phy2.14489.

35. Cantó, C., Jiang, L.Q., Deshmukh, A.S., Mataki, C., Coste, A., Lagouge, M., Zierath, J.R., and Auwerx, J. (2010). Interdependence of AMPK and SIRT1 for Metabolic Adaptation to Fasting and Exercise in Skeletal Muscle. Cell Metab. *11*, 213–219. 10.1016/j.cmet.2010.02.006.

36. Gvozdjáková, A., Sumbalová, Z., Kucharská, J., Komlósi, M., Rausová, Z., Vancová, O., Számosová, M., and Mojto, V. (2020). Platelet mitochondrial respiration, endogenous coenzyme Q10 and oxidative stress in patients with chronic kidney disease. Diagnostics *10*, 1–13. 10.3390/diagnostics10030176.

37. Jin, Z., Zhang, Q., Wondimu, E., Verma, R., Fu, M., Shuang, T., Arif, H.M., Wu, L., and Wang, R. (2020). H2S-stimulated bioenergetics in chicken erythrocytes and the underlying mechanism. Am. J. Physiol. - Regul. Integr. Comp. Physiol. *319*, E69–E78. 10.1152/ajpregu.00348.2019.

38. Malkoc, K., Casagrande, S., and Hau, M. (2021). Inferring whole-organism metabolic rate from red blood cells in birds. Front. Physiol. *12*, 1–11. 10.3389/fphys.2021.691633.

39. Nord, A., Metcalfe, N.B., Page, J.L., Huxtable, A., McCafferty, D.J., and Dawson, N.J. (2021). Avian red blood cell mitochondria produce more heat in winter than in autumn. FASEB J. *35*, 1–12. 10.1096/fj.202100107R.

40. Gangloff, E.J., Schwartz, T.S., Klabacka, R., Huebschman, N., Liu, A.Y., and Bronikowski, A.M. (2020).

Mitochondria as central characters in a complex narrative: Linking genomics, energetics, pace-of-life, and aging in natural populations of garter snakes. Exp. Gerontol. *137*, 110967. 10.1016/j.exger.2020.110967.

41. Salin, K., Auer, S.K., Rudolf, A.M., Anderson, G.J., Selman, C., and Metcalfe, N.B. (2016). Variation in metabolic rate among individuals is related to tissue-specific differences in mitochondrial leak respiration. Physiol. Biochem. Zool. *89*, 511–523. 10.1086/688769.
42. Huang, Z., Gallot, A., Lao, N.T., Puechmaille, S.J., Foley, N.M., Jebb, D., Bekaert, M., and Teeling, E.C. (2016). A nonlethal sampling method to obtain, generate and assemble whole blood transcriptomes from small, wild mammals. Mol. Ecol. Resour. *16*, 150–162. 10.1111/1755-0998.12447.
43. Demanelis, K., Jasmine, F., Chen, L.S., Chernoff, M., Tong, L., Delgado, D., Zhang, C., Shinkle, J., Sabarinathan, M., Lin, H., et al. (2020). Determinants of telomere length across human tissues. Science (80-.). *369*. 10.1126/SCIENCE.AAZ6876.
44. Kim, E., Jung, Y.S., Kim, H., Kim, J.S., Park, M., Jeong, J., Lee, S.K., Yoon, H.G., Hwang, G.S., and Namkoong, K. (2014). Metabolomic signatures in peripheral blood associated with Alzheimer's disease amyloid-β-induced neuroinflammation. J. Alzheimer's Dis. *42*, 421–433. 10.3233/JAD-132165.
45. Klaus, S., and Ost, M. (2020). Mitochondrial uncoupling and longevity – A role for mitokines? Exp. Gerontol. *130*, 110796. 10.1016/j.exger.2019.110796.
46. Margaritelis, N. V., Veskoukis, A.S., Paschalis, V., Vrabas, I.S., Dipla, K., Zafeiridis, A., Kyparos, A., and Nikolaidis, M.G. (2015). Blood reflects tissue oxidative stress: A systematic review. Biomarkers *20*, 97–108. 10.3109/1354750X.2014.1002807.
47. Pandey, K.B., and Rizvi, S.I. (2011). Biomarkers of oxidative stress in red blood cells. Biomed. Pap. *155*, 131–136. 10.5507/bp.2011.027.
48. Picard, M., Juster, R.P., and McEwen, B.S. (2014). Mitochondrial allostatic load puts the "gluc" back in glucocorticoids. Nat. Rev. Endocrinol. *10*, 303–310. 10.1038/nrendo.2014.22.
49. Müller, M.J., Geisler, C., Hübers, M., Pourhassan, M., and Braun, W. (2018). Normalizing resting energy expenditure across the life course in humans : challenges and hopes. Eur. J. Clin. Nutr., 628–637. 10.1038/s41430-018-0151-9.
50. Karamercan, M.A., Weiss, S.L., Villarroel, J.P.P., Guan, Y., Werlin, E., Figueredo, R., Becker, L.B., and Sims, C. (2013). Can peripheral blood mononuclear cells be used as a proxy for mitochondrial dysfunction in vital organs during hemorrhagic shock and resuscitation? Shock *40*, 476–484. 10.1097/SHK.0000000000000026.
51. Divakaruni, A.S., and Jastroch, M. (2022). A practical guide for the analysis, standardization and interpretation of oxygen consumption measurements. Nat. Metab. *4*. 10.1038/s42255-022-00619-4.
52. Zaytsoff, S.J.M., Brown, C.L.J., Montina, T., Metz, G.A.S., Abbott, D.W., Uwiera, R.R.E., and Inglis, G.D. (2019). Corticosterone-mediated physiological stress modulates hepatic lipid metabolism, metabolite profiles, and systemic responses in chickens. Sci. Rep. *9*, 1–13. 10.1038/s41598-019-52267-6.
53. Hau, M., Casagrande, S., Ouyang, J.Q., and Baugh, A.T. (2016). Glucocorticoid-Mediated Phenotypes in Vertebrates: Multilevel Variation and Evolution. Adv. Study Behav. *48*, 41–115.

10.1016/bs.asb.2016.01.002.

54. De Bruijn, R., and Romero, L.M. (2013). Artificial rain and cold wind act as stressors to captive molting and non-molting European starlings (Sturnus vulgaris). Comp. Biochem. Physiol. - A Mol. Integr. Physiol. *164*, 512–519. 10.1016/j.cbpa.2012.12.017.

55. Fowler, M.A., and Williams, T.D. (2017). A physiological signature of the cost of reproduction associated with parental care. Am. Nat. *190*, 762–773. 10.1086/694123.

56. Love, O.P., Breuner, C.W., Vézina, F., and Williams, T.D. (2004). Mediation of a corticosterone-induced reproductive conflict. Horm. Behav. *46*, 59–65. 10.1016/j.yhbeh.2004.02.001.

57. Casagrande, S., Demoranville, K.J., Trost, L., Pierce, B., Bryła, A., Dzialo, M., Sadowska, E.T., Bauchinger, U., and McWilliams, S.R. (2020). Dietary antioxidants attenuate the endocrine stress response during long-duration flight of a migratory bird: Anthocyanins lower corticosterone rise. Proc. R. Soc. B Biol. Sci. *287*. 10.1098/rspb.2020.0744rspb20200744.

58. Hill, G.E., Hood, W.R., Ge, Z., Grinter, R., Greening, C., Johnson, J.D., Park, N.R., Taylor, H.A., Andreasen, V.A., Powers, M.J., et al. (2019). Plumage redness signals mitochondrial function in the house finch. Proc. R. Soc. B Biol. Sci. *286*. 10.1098/rspb.2019.1354.

59. Heymsfield, S.B., Peterson, C.M., Bourgeois, B., Thomas, D.M., Gallagher, D., Strauss, B., Müller, M.J., and Bosy-Westphal, A. (2018). Human energy expenditure: advances in organ-tissue prediction models. Obes. Rev. *19*, 1177–1188. 10.1111/obr.12718.

60. Fernández-Verdejo, R., and Galgani, J.E. (2022). Predictive equations for energy expenditure in adult humans: From resting to free-living conditions. Obesity *30*, 1537–1548. 10.1002/oby.23469.

61. Konarzewski, M., and Diamond, J. (1995). Evolution of basal metabolic rate and organ masses in laboratory mice. Evolution (N. Y). *49*, 1239–1248.

62. Chappel, M.A., Bech, C., and A., B.W. (1999). The relationship of central and peripheral organ masses to aerobic performance variation in house sparrows. J. Exp. Biol. *2279*, 2269–2279.

63. Sabounchi, N.S., Rahmandad, H., and Ammerman, A. (2013). Best-fitting prediction equations for basal metabolic rate: Informing obesity interventions in diverse populations. Int. J. Obes. *37*, 1364–1370. 10.1038/ijo.2012.218.

64. Gödecke, A., and Haendeler, J. (2017). Intra- and interorgan communication in the cardiovascular system: A special view on redox regulation. Antioxidants Redox Signal. *26*, 613–615. 10.1089/ars.2017.6988.

65. Sutendra, G., and Michelakis, E.D. (2014). The metabolic basis of pulmonary arterial hypertension. Cell Metab. *19*, 558–573. 10.1016/j.cmet.2014.01.004.

66. McWilliams, S., Pierce, B., Wittenzellner, A., Langlois, L., Engel, S., Speakman, J.R., Fatica, O., Demoranville, K., Goymann, W., Trost, L., et al. (2020). The energy savings-oxidative cost trade-off for migratory birds during endurance flight. Elife *9*, 1–18. 10.7554/eLife.60626.

67. Biebach, H. (1984). Effect of clutch size and time of day on the energy expenditure of incubating starlings (Sturnus vulgaris). Physiol. Zool. *57*, 26–31.

68. Clark, A.L. (1987). Thermal constraints on foraging in adult European starlings. Oecologia *71*, 233–238.

69. Scott, I., and Evans, P.R. (1992). The metabolic output of avian (Sturnus vulgaris, Calidris alpina) adipose tissue, liver, and skeletal muscle: implications for BMR/body mass relationships. Comp Biochem Physiol *103*, 329–332.

70. Pesta, D., and Gnaiger, E. (2012). High-resolution respirometry: OXPHOS protocols for human cells and permeabilized fibers from small biopsies of human muscle T. R. Figueira, D. R. Melo, A. E. Vercesi, and R. F. Castilho, eds. 10.1007/978-1-61779-382-0.

71. Goodrich B, J, G., I, A., and Brilleman, S. (2023). rstanarm: Bayesian applied regression modeling via Stan.". R Packag. version 2.21.4, https//mc-stan.org/rstanarm/.

72. Korner-Nievergelt, F., Roth, T., von Felten, S., Guélat, J., Almasi, B., and Korner-Nievergelt, P. (2015). Model Selection and Multimodel Inference. Bayesian Data Anal. Ecol. Using Linear Model. with R, BUGS, STAN, 175–196. 10.1016/b978-0-12-801370-0.00011-3.

73. Heidelberger, P., and Welch, P. (1983). Simulation run length control in the presence of an initial transient. Opns Res *31*, 1109–1144.

74. McElreath, R. (2020). Statistical Rethinking. A Bayesian Course with Examples in R and Stan second. (Chapman and Hall/CRC).

75. Levine, M.E., Lu, A.T., Quach, A., Chen, B.H., Assimes, T.L., Bandinelli, S., Hou, L., Baccarelli, A.A., Stewart, J.D., Li, Y., et al. (2018). No TitleAn epigenetic biomarker of aging for lifespan and healthspan. Aging (Albany. NY). *10*, 573–591.

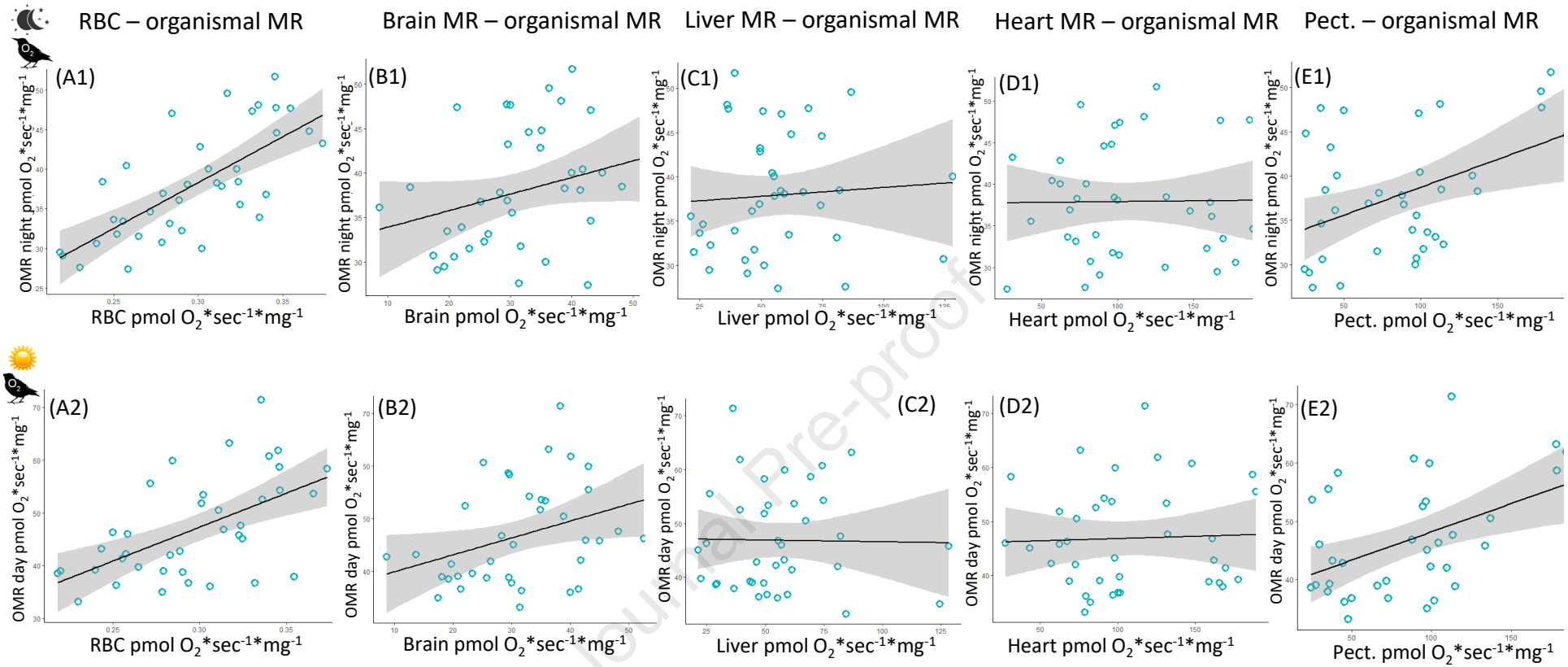

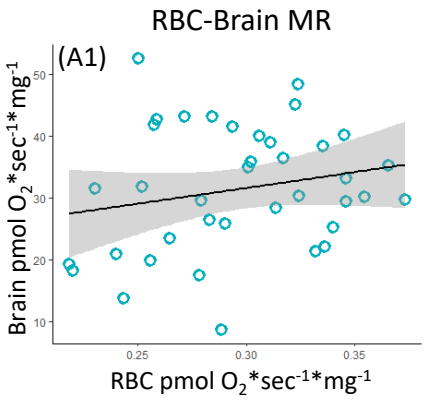

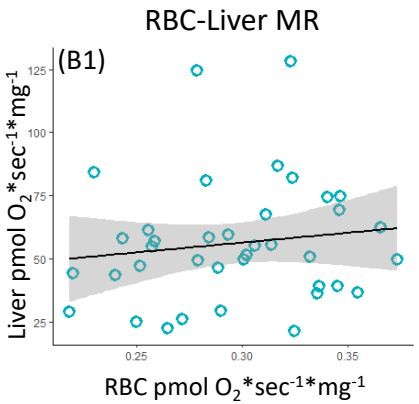

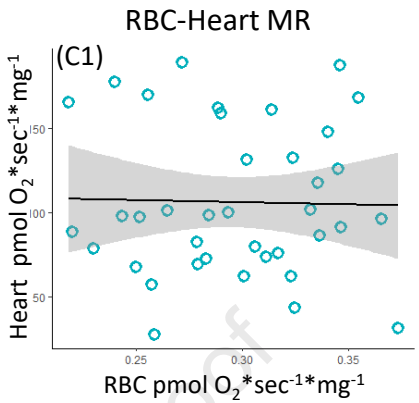

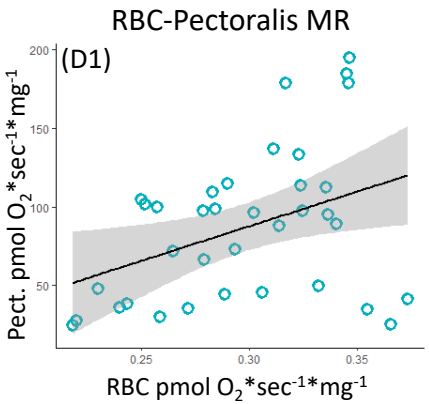

- Tools to measure energy metabolism in free-ranging animals are limited
- We examined metabolic rate (MR) of bird tissues as potential proxy for organism MR
- Blood predicted whole-organism MR better than pectoralis, heart, brain and liver
- Blood MR gauges use of whole bird energy needs with quick and minimal invasiveness

TABLE FOR AUTHOR TO COMPLETE

Please upload the completed table as a separate document. ***Please do not add subheadings to the key resources table.*** *If you wish to make an entry that does not fall into one of the subheadings below, please contact your handling editor.* ***Any subheadings not relevant to your study can be skipped.*** *(**NOTE:** References within the KRT should be in numbered style rather than Harvard.)*

Key resources table

REAGENT or RESOURCE	SOURCE	IDENTIFIER
Antibodies		
Bacterial and virus strains		
Biological samples		
Chemicals, peptides, and recombinant proteins		
Critical commercial assays		
Deposited data		
Data associated with the study	Mendeley repository	https://data.mendeley.com/drafts/752nyp5j2n

Experimental models: Cell lines		
Experimental models: Organisms/strains		
5-year-old male captive European starlings (*Sturnus vulgaris*)	Wild-caught	NA
Oligonucleotides		
Recombinant DNA		
Software and algorithms		
Other		

LIFE SCIENCE TABLE WITH EXAMPLES FOR AUTHOR REFERENCE

REAGENT or RESOURCE	SOURCE	IDENTIFIER
Antibodies		
Rabbit monoclonal anti-Snail	Cell Signaling Technology	Cat#3879S; RRID: AB_2255011
Mouse monoclonal anti-Tubulin (clone DM1A)	Sigma-Aldrich	Cat#T9026; RRID: AB_477593
Rabbit polyclonal anti-BMAL1	This paper	N/A
Bacterial and virus strains		
pAAV-hSyn-DIO-hM3D(Gq)-mCherry	Krashes et al.[1]	Addgene AAV5; 44361-AAV5
AAV5-EF1a-DIO-hChR2(H134R)-EYFP	Hope Center Viral Vectors Core	N/A
Cowpox virus Brighton Red	BEI Resources	NR-88
Zika-SMGC-1, GENBANK: KX266255	Isolated from patient (Wang et al.[2])	N/A
Staphylococcus aureus	ATCC	ATCC 29213
Streptococcus pyogenes: M1 serotype strain: strain SF370; M1 GAS	ATCC	ATCC 700294
Biological samples		
Healthy adult BA9 brain tissue	University of Maryland Brain & Tissue Bank; http://medschool.umaryland.edu/btbank/	Cat#UMB1455
Human hippocampal brain blocks	New York Brain Bank	http://nybb.hs.columbia.edu/
Patient-derived xenografts (PDX)	Children's Oncology Group Cell Culture and Xenograft Repository	http://cogcell.org/
Chemicals, peptides, and recombinant proteins		
MK-2206 AKT inhibitor	Selleck Chemicals	S1078; CAS: 1032350-13-2
SB-505124	Sigma-Aldrich	S4696; CAS: 694433-59-5 (free base)
Picrotoxin	Sigma-Aldrich	P1675; CAS: 124-87-8
Human TGF-β	R&D	240-B; GenPept: P01137
Activated S6K1	Millipore	Cat#14-486
GST-BMAL1	Novus	Cat#H00000406-P01
Critical commercial assays		
EasyTag EXPRESS 35S Protein Labeling Kit	PerkinElmer	NEG772014MC
CaspaseGlo 3/7	Promega	G8090
TruSeq ChIP Sample Prep Kit	Illumina	IP-202-1012
Deposited data		
Raw and analyzed data	This paper	GEO: GSE63473
B-RAF RBD (apo) structure	This paper	PDB: 5J17

Human reference genome NCBI build 37, GRCh37	Genome Reference Consortium	http://www.ncbi.nlm.nih.gov/projects/genome/assembly/grc/human/
Nanog STILT inference	This paper; Mendeley Data	http://dx.doi.org/10.17632/wx6s4mj7s8.2
Affinity-based mass spectrometry performed with 57 genes	This paper; Mendeley Data	Table S8; http://dx.doi.org/10.17632/5hvpvspw82.1
Experimental models: Cell lines		
Hamster: CHO cells	ATCC	CRL-11268
D. melanogaster: Cell line S2: S2-DRSC	Laboratory of Norbert Perrimon	FlyBase: FBtc0000181
Human: Passage 40 H9 ES cells	MSKCC stem cell core facility	N/A
Human: HUES 8 hESC line (NIH approval number NIHhESC-09-0021)	HSCI iPS Core	hES Cell Line: HUES-8
Experimental models: Organisms/strains		
C. elegans: Strain BC4011: srl-1(s2500) II; dpy-18(e364) III; unc-46(e177)rol-3(s1040) V.	Caenorhabditis Genetics Center	WB Strain: BC4011; WormBase: WBVar00241916
D. melanogaster: RNAi of Sxl: y[1] sc[*] v[1]; P{TRiP.HMS00609}attP2	Bloomington Drosophila Stock Center	BDSC:34393; FlyBase: FBtp0064874
S. cerevisiae: Strain background: W303	ATCC	ATTC: 208353
Mouse: R6/2: B6CBA-Tg(HDexon1)62Gpb/3J	The Jackson Laboratory	JAX: 006494
Mouse: OXTRfl/fl: B6.129(SJL)-Oxtr$^{tm1.1Wsy}$/J	The Jackson Laboratory	RRID: IMSR_JAX:008471
Zebrafish: Tg(Shha:GFP)t10: t10Tg	Neumann and Nuesslein-Volhard[3]	ZFIN: ZDB-GENO-060207-1
Arabidopsis: 35S::PIF4-YFP, BZR1-CFP	Wang et al.[4]	N/A
Arabidopsis: JYB1021.2: pS24(AT5G58010)::cS24:GFP(-G):NOS #1	NASC	NASC ID: N70450
Oligonucleotides		
siRNA targeting sequence: PIP5K I alpha #1: ACACAGUACUCAGUUGAUA	This paper	N/A
Primers for XX, see Table SX	This paper	N/A
Primer: GFP/YFP/CFP Forward: GCACGACTTCTTCAAGTCCGCCATGCC	This paper	N/A
Morpholino: MO-pax2a GGTCTGCTTTGCAGTGAATATCCAT	Gene Tools	ZFIN: ZDB-MRPHLNO-061106-5
ACTB (hs01060665_g1)	Life Technologies	Cat#4331182
RNA sequence: hnRNPA1_ligand: UAGGGACUUAGGGUUCUCUCUAGGGACUUAGGGUUCUCUCUAGGGA	This paper	N/A
Recombinant DNA		
pLVX-Tight-Puro (TetOn)	Clonetech	Cat#632162
Plasmid: GFP-Nito	This paper	N/A

cDNA GH111110	Drosophila Genomics Resource Center	DGRC:5666; FlyBase:FBcl0130415
AAV2/1-hsyn-GCaMP6- WPRE	Chen et al.[5]	N/A
Mouse raptor: pLKO mouse shRNA 1 raptor	Thoreen et al.[6]	Addgene Plasmid #21339
Software and algorithms		
ImageJ	Schneider et al.[7]	https://imagej.nih.gov/ij/
Bowtie2	Langmead and Salzberg[8]	http://bowtie-bio.sourceforge.net/bowtie2/index.shtml
Samtools	Li et al.[9]	http://samtools.sourceforge.net/
Weighted Maximal Information Component Analysis v0.9	Rau et al.[10]	https://github.com/ChristophRau/wMICA
ICS algorithm	This paper; Mendeley Data	http://dx.doi.org/10.17632/5hvpvspw82.1
Other		
Sequence data, analyses, and resources related to the ultra-deep sequencing of the AML31 tumor, relapse, and matched normal	This paper	http://aml31.genome.wustl.edu
Resource website for the AML31 publication	This paper	https://github.com/chrisamiller/aml31SuppSite

PHYSICAL SCIENCE TABLE WITH EXAMPLES FOR AUTHOR REFERENCE

REAGENT or RESOURCE	SOURCE	IDENTIFIER
Chemicals, peptides, and recombinant proteins		
QD605 streptavidin conjugated quantum dot	Thermo Fisher Scientific	Cat#Q10101MP
Platinum black	Sigma-Aldrich	Cat#205915
Sodium formate BioUltra, ≥99.0% (NT)	Sigma-Aldrich	Cat#71359
Chloramphenicol	Sigma-Aldrich	Cat#C0378
Carbon dioxide (^{13}C, 99%) (<2% ^{18}O)	Cambridge Isotope Laboratories	CLM-185-5
Poly(vinylidene fluoride-co-hexafluoropropylene)	Sigma-Aldrich	427179
PTFE Hydrophilic Membrane Filters, 0.22 μm, 90 mm	Scientificfilters.com/Tisch Scientific	SF13842
Critical commercial assays		
Folic Acid (FA) ELISA kit	Alpha Diagnostic International	Cat# 0365-0B9
TMT10plex Isobaric Label Reagent Set	Thermo Fisher	A37725
Surface Plasmon Resonance CM5 kit	GE Healthcare	Cat#29104988
NanoBRET Target Engagement K-5 kit	Promega	Cat#N2500
Deposited data		
B-RAF RBD (apo) structure	This paper	PDB: 5J17
Structure of compound 5	This paper; Cambridge Crystallographic Data Center	CCDC: 2016466
Code for constraints-based modeling and analysis of autotrophic *E. coli*	This paper	https://gitlab.com/elad.noor/sloppy/tree/master/rubisco
Software and algorithms		
Gaussian09	Frish et al.[1]	https://gaussian.com
Python version 2.7	Python Software Foundation	https://www.python.org
ChemDraw Professional 18.0	PerkinElmer	https://www.perkinelmer.com/category/chemdraw
Weighted Maximal Information Component Analysis v0.9	Rau et al.[2]	https://github.com/ChristophRau/wMICA
Other		
DASGIP MX4/4 Gas Mixing Module for 4 Vessels with a Mass Flow Controller	Eppendorf	Cat#76DGMX44
Agilent 1200 series HPLC	Agilent Technologies	https://www.agilent.com/en/products/liquid-chromatography
PHI Quantera II XPS	ULVAC-PHI, Inc.	https://www.ulvac-phi.com/en/products/xps/phi-quantera-ii/